Retrieving structural information from scattering and attenuation data of transparent wood and (Nano)paper

Yoshiharu Nishiyama

Journal of Bioresources and Bioproducts 6 (2021) 187–194

Contents lists available at ScienceDirect

Journal of Bioresources and Bioproducts

journal homepage: www.elsevier.com/locate/jobab

Retrieving structural information from scattering and attenuation data of transparent wood and (Nano)paper

Yoshiharu Nishiyama

Univ. Grenoble Alpes, CNRS, CERMAV, Grenoble, 38000, France

ARTICLE INFO

Keywords:
Light scattering
Transparent wood
Nanocellulose

ABSTRACT

Over the last 15 years, significant number of reports on transparent paper and transparent wood appeared in the literature. The light scattering data or transmission data are often given to describe the optical performance of the material. In addition, the data also contains structural information that can be further analyzed based on scattering theory. Some of the data are re-analyzed herein from structural analysis point of view related to the scattering phenomena. Quantitative analysis on the wavelength dependent optical density of nanopaper suggested that the scatterers are not isolated voids or microfibrils but rather large submicrometric and structural domains. Angular dependence of transparent wood scattering suggests the scattering units of a few micrometers such as cell wall are at the origin of high haze.

1. Introduction

Seeing through a relatively thick piece of wood is not in our daily experience, and thus strike our mind. Part of the popularity of “transparent paper” and “transparent wood” in recent days in scientific journals is due to the surprise effect to reveal properties not expected in our daily observation. Yet they are based on the same physics as the one behind our daily experience of seeing wood turning to deeper color when wet with water or put wax or see our paper translucent when put some oil.

We see deeper color when wood surface is wet, because the light penetrates deeper before scattering back losing some of the color components absorbed by chromophores. Paper becomes translucent when wet because the light is scattered less. Three ingredients are at play: 1) structure (morphology), 2) refractive index and 3) absorption. To fully understand the optical property and have control over it, we should decouple the three effect.

Is it possible to further suppress diffusion? Is there any limit in transparency? What are the contribution of different structure levels to the light scattering? Here we should try to get some hints from the data in the literature.

2. Rayleigh scattering

Rayleigh scattering is responsible for the blue sky we see in the daytime and reddish dawn or sunsets. Small molecules or particles, much smaller than the wavelength of visible light, in the atmosphere are indeed scattering light, whose scattering power depends on wavelength and the size of particles. In such cases, unpolarized light is scattered isotropically in all direction simply proportional to $(1+\cos 2\theta)/2$ and to λ^{-4}, where θ is the scattering angle and λ the wavelength. Studying the scattering allows us to investigate the size or concentration of the particles in such case, and to provide the basis of molecular weight determination.

However, measuring static light scattering of turbid system is problematic because the photons scatter many times before entering the detector. One workaround in turbid system is to rely on wavelength-dependent turbidity measurement, as was already treated for atmosphere by Rayleigh (1899), and further developed by Debye (1944) on solution. In turbidity measurement, it will be exceptional

E-mail address: yoshiharu.nishiyama@cermav.cnrs.fr

https://doi.org/10.1016/j.jobab.2021.05.001

Available online 24 May 2021

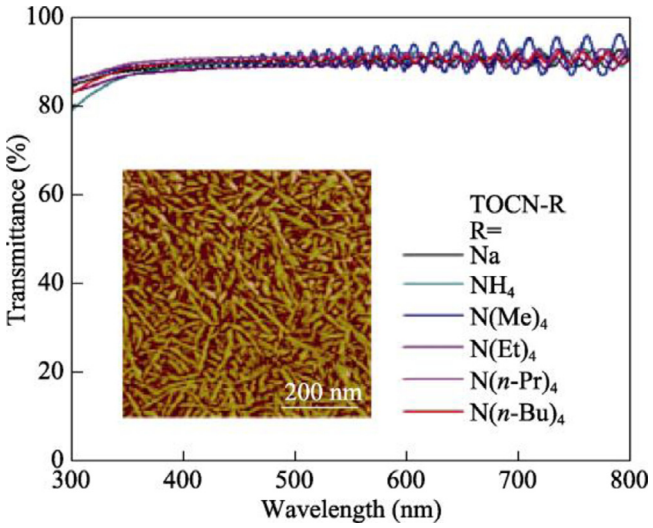

Fig. 1. Transmission spectra of thin (10 μm) film of TEMPO oxidized nanocellulose film ion exchanged with quaternary ammoniums. Reproduced from Shimizu et al. (2014).

to harvest a photon after multiple scattering. Hence the scattering theory of dilute system is also applicable in relatively concentrated system if we just measure turbidity as a function of wavelength, or regular transmission.

Integrating over the scattered intensity over the whole direction would be equivalent of the intensity loss, and thus, the turbidity τ can be obtained as:

$$\tau = \frac{32\pi^2}{3}\frac{n_o^2(\bar{n}-n_0)^2}{\lambda^4}\frac{1}{N} \tag{1}$$

where N is the number density of scatterer, n_o is the refractive index of the solvent and $\bar{n}$ is the refractive index of the solution. This can be further rewritten as:

$$\tau = \frac{32\pi^2}{3}\frac{n_o^2(n_1-n_0)^2}{\lambda^4}\phi v \tag{2}$$

where n_1 is the refractive index of particle and ϕ is the volume fraction of scatterer, and v is the volume of each scatterer.

Similarly, for long object suspended in a medium, Carr and Hermans (1978) derived the turbidity expression, which leads to

$$\tau = \frac{88\pi^3\bar{n}}{15\lambda^3}(n_1-n_0)^2\phi a \tag{3}$$

after rearrangement. Here a is the cross-sectional area of the fibrillar object. We used this behavior to characterize cellulose suspensions (Shimizu et al., 2016; Tanaka et al., 2017). These equations hold true even for solid, as it is not related to the dynamics of the material. The turbidity data can be collected from solid sample by just replacing the sample cuvette of standard UV-vis spectrometer. This kind of measurements are reported by the group of Professor Isogai and Saito (using the most standard equipment in a chemistry laboratory), on thin films of TEMPO oxidized nanocelluose. For example, spectra by Shimizu et al. (2014) are reproduced here in Fig. 1.

A quick inspection of the spectra shows fringes and slightly reduced transmittance at lower wavelength and an average transmission of 90%. The fringe in the transmission spectra is due to the thin film interference, whose transmission as function of thickness d, simplified from Swanepoel (1983), is

$$T(d) = \frac{16n^2}{A - 2(n^2-1)^2\cos(4\pi nd/\lambda)} \tag{4}$$

where

$$A = (n+1)^4 + (n-1)^4 \tag{5}$$

In this function, the fringe maximum is always 100%, but we introduce some variation in the thickness of probed area with standard deviation σ such that

$$T(d,\sigma) = \int \frac{1}{\sqrt{2\pi\sigma}}\exp\left(-\left(\frac{x}{2\sigma}\right)^2\right)T(d+x)dx \tag{6}$$

If the film contains scatterer such as voids or fibrils, much smaller than the wavelength, Rayleigh scattering contribution leads to further decrease in transmission such that

$$T_{\text{total}} = T(d,\sigma)\exp(-\tau d) \tag{7}$$

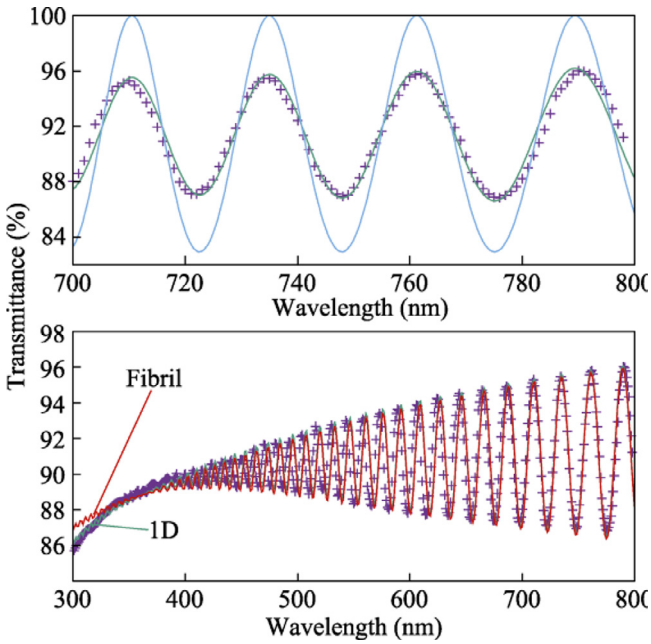

Fig. 2. Fit to the transmission data of $N(Me)_4$, blue: using Eq. (4), green: using Eqs (7) and (2), red: using Eqs (7) and (3).

Fig. 2 shows the zoom up of the transmission data of film with tetramethylammonium in Fig. 1 that showed the highest fringe feature, overlapped with least-square fitted theoretical curves. If the film had perfectly homogeneous thickness, one expect a transmission that reach 100% at the periodic peaks (blue line). Introducing Gaussian distribution of thickness (Eq. (6)) reproduced the attenuated fringe feature (green line), that further attenuates towards lower wavelength (Fig. 2, bottom). In this particular case, the average thickness was fitted to be (6.86 ± 0.04) μm, with a standard deviation of thickness of 65 nm and the global refractive index of 1.551 ± 0.009. The refractive index exactly matches the value given in the report based on Abbe refractometer measurement.

A closer inspection shows discrepancy in the phase of fringes at different wavelengths that can be further fitted by wavelength dependence using Cauchy's formula:

$$n = A + \frac{B}{\lambda^2} \tag{8}$$

but this leads to a non-realistic negative B and might be due to measurement artefacts. It shows at least if precise measurement of wavelength dependent transmission, both film thickness and wavelength dependent refractive index can be fitted with high accuracy.

Now the lowered transmittance at shorter wavelength can be fitted by using Eq. (2) (green line in Fig. 2) bottom or using Eq. (3) (red line). If we consider that the voids that are probably filled with condensed water is at the origin of scattering, the moisture content of this particular sample was 8.1% so we can assume a volume fraction of scatterer $\phi = 0.12$. Putting $n_1 = 1.333$ for water:

$$n_0 = \frac{\bar{n} - \phi n_1}{1 - \phi} = 1.58 \tag{9}$$

Under these hypotheses, the average volume of each scatterer in Eq. (2) can be uniquely determined from the fit as $37{\times}10^3$ nm^3 equivalent to a sphere with a radius of 21 nm. This size is indeed much smaller than the wavelength of visible light, but is much larger than what the atomic force microscopic image in the insert would suggest. Even if the voids are not filled with water, the contrast would only increase by a factor of 5, leading to the expected radius of less than by a factor of two and remains unrealistic. Besides, the porosity of the sample is very low, and the pore diameter measured by the authors with positron annihilation spectroscopy was 0.5 nm

Similarly, if we consider that it comes from fibrillar objects, a source of scattering can be the birefringence of single fibrils of 0.08. Assuming $\phi = 1$, Eq. (3) gives lower estimate of cross-section of 105 nm^2, again too high for a single nanofibers that has a cross section below 10 nm^2.

Then what is scattering light inside the film? The available data so far is not enough to tell the exact nature of the entity responsible for the scattering, since the size, fraction and refractive contrast all contributes to one scalar value of turbidity. The transmission spectra still tell us that a submicrometric fluctuation at larger scale than 50 nm probably exists. Since the fit to the experiment corresponds to:

$$(\Delta n)^2 \phi v \approx 273 \left[nm^3\right] \tag{10}$$

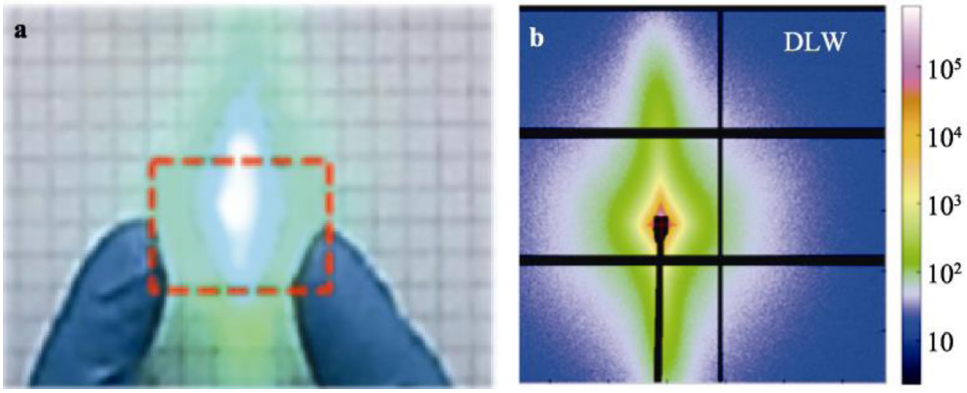

Fig. 3. a: Laser light scattering image of transparent wood and b: X-ray scattering image of delignified wood. The long axis is horizontal in both cases. Both images reproduced from Li et al. (2016).

We can do a back-of-the-envelope calculation about the implication of the value. For patches with 100 nm in radius, taking $\phi = 1$ the contrast can be as low as 0.008 or one tenth of intrinsic birefringence of crystalline cellulose (Iyer et al., 1968). Relatively large sub-micrometric fluctuation with small refractive index contrast would explain the scattering feature of this sample.

3. Small angle scattering at different length scales

Wood-based material has been also studied by X-ray and neutron scattering. The phenomena behind are described with almost the same formalism, though we do not see the consequence by our naked eyes, and instead obliged to use detectors. Typical wavelength of X-ray and neutron used in scattering experiment are 0.5–2 Å while visible lights are in the 500 nm range, so there is roughly ten thousand times difference in the length scale. As wood or cellulose materials are in general anisotropic at all length scales, the scattering is orientation dependent, as the visual similarity of laser light scattering pattern and X-ray scattering pattern shown by Li et al. (2016) (Fig. 3).

In both cases, a similar qualitative explanation can be given. The light scattering and X-ray/neutron scattering are due to the refractive index/electron density/neutron scattering length density fluctuation. For example, wood cell wall is constituted of crystalline cellulose microfibril mostly aligned parallel to the long axis embedded in matrix components. This gives rise to fluctuation of electron density or neutron scattering length density perpendicular to the fiber axis at a length scale above a few nanometers. This fluctuation is at the origin of the small angle scattering of X-ray or neutron at sub-nanometer length scale. The scattering is stronger perpendicular to the fiber axis because this is the direction of density fluctuation.

At higher length scale, wood is packed with elongated cell of 20–50 μm, again mostly aligned parallel along the trunk or branch of a tree. When probed with a light of sub-micrometer wavelength (visible regime) stronger scattering is seen perpendicular to the fiber direction. In general, even for “transparent wood”, visible light scatters much more than X-ray: in Fig. 3a, the direct laser point is not present since all photons are scattered at least once, whereas, and beamstop is needed for X-ray diffraction measurement to protect the screen as most of the X-ray photons go straight through the sample without being scattered by the sample.

Since the scattering of the electromagnetic wave (visible light/X-ray) and particle wave (neutron) is due to the interference between the waves emitted by different components of the sample, the scattering can be related to the structure by simple Fourier transform. The scattering data does not give directly the three-dimensional structure but give structure-related parameters in a relatively straightforward way.

4. Multiple scattering

When analyzing the scattering in quantitative manner, one obstacle for light scattering would be multiple scattering. In a typical X-ray scattering, the direct beam is mainly attenuated by photo-electric absorption, and most photons are scattered only once before entering the detector. Thus the scattered intensity is simply proportional to the sample thickness, and the scattering profile does not change its shape as function of sample thickness.

In a strongly scattering situation, this condition does not necessarily hold. Indeed, Vasileva et al. (2018) showed that the angular dependency of scattered light intensity drastically changes with thickness (Fig. 4).

This can be understood in the following way. If a scattering feature of infinitesimal thickness of the sample dt as function of angle θ is given as $f(\theta)$, the incident beam I_0 is decreased by $I_0 \int 2\pi \sin\theta f(\theta) \mathrm{d}\theta$, or for anisotropic case, over the solid angle $\int_S f(\Omega)\mathrm{d}\Omega$ for anisotropic case, and thus for any solid angle Ω:

$$\frac{\mathrm{d}I(\Omega)}{\mathrm{d}t} = \int_S I(\Omega+\omega) f(-\omega)\mathrm{d}\omega - I(\Omega)\int_S f(\omega-\Omega)\mathrm{d}\omega \tag{11}$$

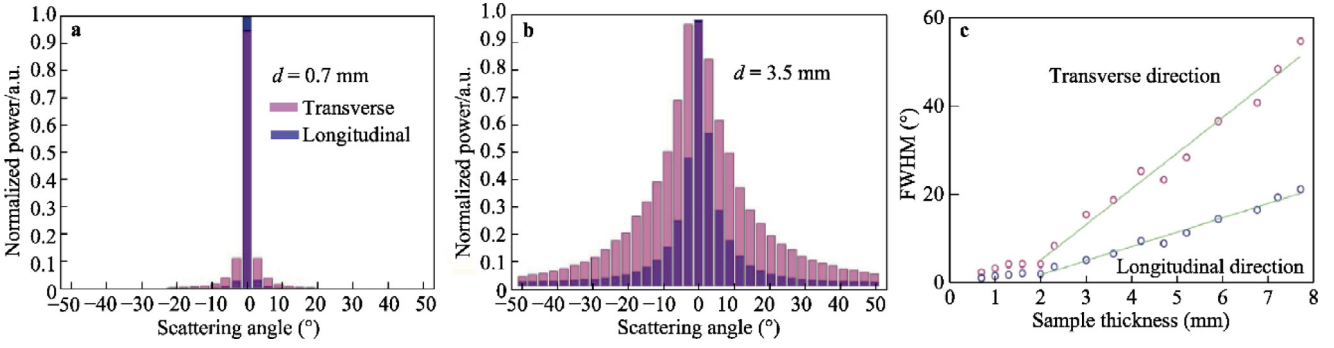

Fig. 4. a, b: Laser light scattering intensity of transparent wood in the direction along (purple) and perpendicular (red) to the longitudinal direction as function of scattering angle. The sample thickness was 0.7 mm for *a* and 3.5 nn for *b*; c: the full width at half maximum (FWHM) of the laser light scattering intensity profile as function of sample thickness. Arranged from Vasileva et al. (2018).

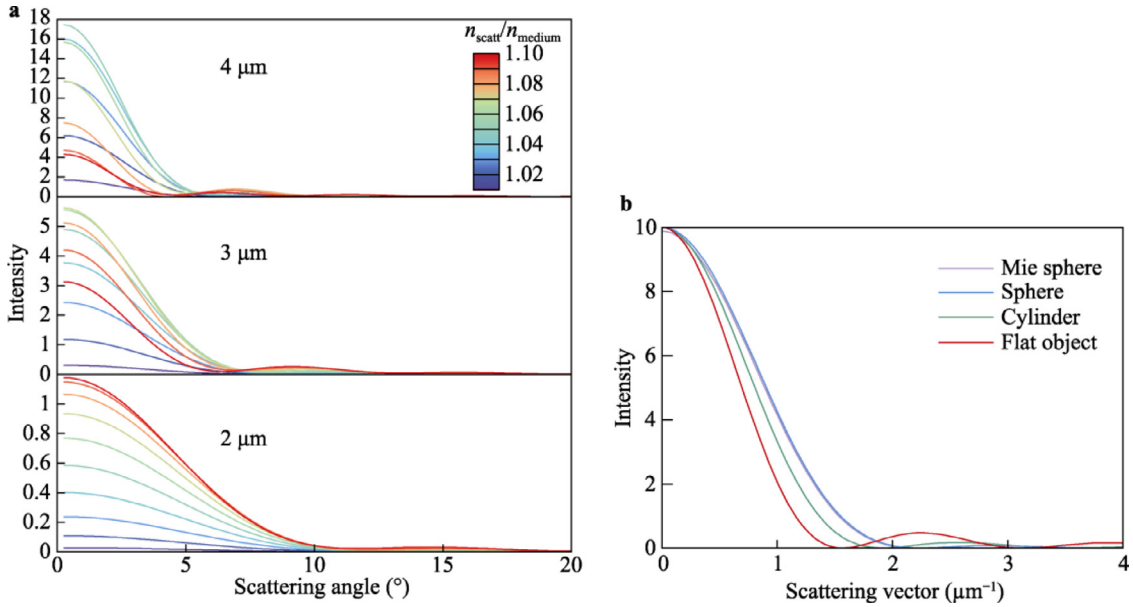

Fig. 5. a, simulated scattering based on program by Bohren and Huffman (1983) on Mie scattering of spheres of radius 2 μm, 3 μm and 4μm with various refractive index ratio to the continuous phase; b, intensity based on form factors for X-ray/neutron scattering sphere: $I = [\frac{3}{qr}(\frac{\sin(qr)}{(qr)^2} - \frac{\cos(qr)}{qr})]^2$, cylinder perpendicular to the long axis: $I = (\frac{2J_1(qr)}{qr})^2$and platelet perpendicular to the plate: $I = (\frac{\sin(qr)}{qr})^2$for radius $r = 2$.

and each scattered beam in turn behaves as incident beam in the following thickness. As far as $I(0)$ is dominant compared with $I(\Omega \neq 0)$, the observed scattering intensity distribution is directly reflecting the scattering function $f(\theta)$. However, the second term contributes to the decrease in the incident beam intensity, and when scattered intensity becomes important with respect to the incident beam, the angular profile b broadens. The fact that the width of the scattering intensity profile increases proportionally to the thickness can be understood intuitively from the fact that convolution of two Gaussian functions is a Gaussian function with the width being the sum of two widths (Weisstein, E.W. "Convolution." from mathworld—a wolfram web resource. Available at: https://mathworld.wolfram.com/Convolution.html.).

5. Origin of the forward scattering

Now with the multiple scattering the analysis seems complex, but can we still derive some information on the size of the scatterer? Comparison of Fig. 4a and b indicates that incident beam is still major part at 0.7 mm width at this resolution) while at 3.5 mm thickness, there is no sign of direct beam. Thus the signal out of the central positions are probably scattered by single scattering event. If we neglect the central beam, the width of this component seems to have roughly a full width at half maximum of 10°.

Fig. 5a shows the scattering profile calculated for spheres with radius of 2–4 μm using Mie scattering calculation based on the program by Bohren and Huffman (1983) as function of angle for a wavelength of 633 nm. The refractive index n_{scatt} with respect to the refractive index of the continuous phase n_{medium} was also varied as n_{scatt}/n_{medium} of 1.01 to 1.1. For small sphere, the scattering intensity monotonically increased with the refractive index of the scatterer in this range, but for larger sphere, the scattering intensity is not monotonically increasing. This is because phase difference becomes significant over the size of the wavelength: 10% reduction of wavelength over 6 μm results in about 2π phase difference for a 633 nm light.

For smaller sphere or smaller change in refractive index, we do not have to consider the wavelength change inside the scattering body, and thus a simple analytical form factor sufficiently describes the scattering as shown in Fig. 5b, where the sphere simulation is exactly superposed with sphere scattering function (Guinier and Fournet, 1955).

$$I = \left[\frac{3}{qr}\left(\frac{\sin(qr)}{(qr)^2} - \frac{\cos(qr)}{qr}\right)\right]^2 \tag{12}$$

where the scattering vector $q = 4\pi\sin\theta/\lambda$ and θ is half the scattering angle, λ is the wavelength of light (633 nm). Analytical scattering function for infinite cylinder with radius of 2 in the direction perpendicular to the long axis, as well as platelet with thickness of 4 are also shown in the same graph, that gives roughly similar feature in the small angle.

The comparison of the observed scattering features and the simulation would indicate that the scattering entity in this particular balsa would have a dimension of roughly 5 μm, much smaller than the size of a cell, but corresponding to rather the cell wall thickness or cell corners. It would be interesting to compare scattering of other types of wood to see correlation between cell wall thickness and the scattering features.

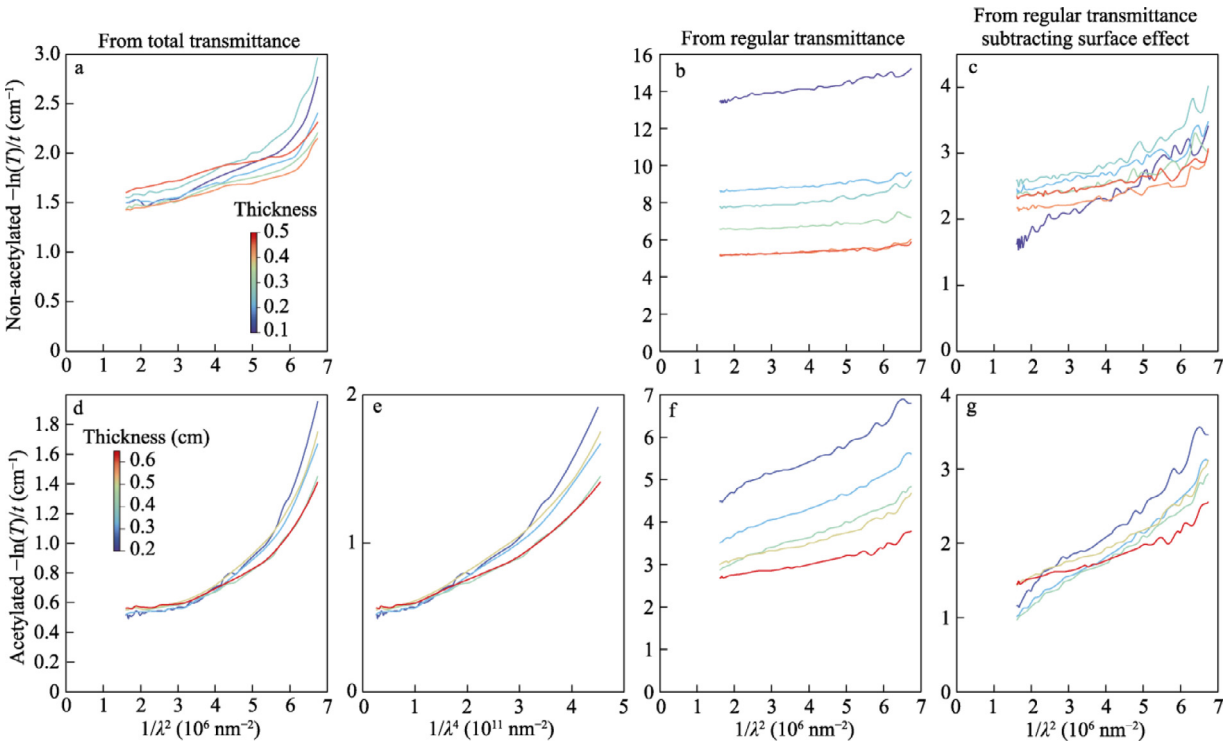

Fig. 6. Normalized turbidity of transparent wood as function of wavelength, data taken from Chen et al. (2019). a–c: non-aceetylated transparent wood, d–g: acetylated transparent wood; a, d: calculated from total transmittance plotted against $1/\lambda^2$, e: against $1/\lambda^4$, b, f: calculated from regular transmittance excluding forward scattering; c, g: same as b, f but normalized after subtracting a constant value.

6. Turbidimetry of transparent wood

Chen et al. (2019) reports the apparent linearity of optical thickness:

$$\tau_{\text{total}} = -\ln(T_{\text{total}}) \tag{13}$$

of the transparent wood as function of sample thickness using the total transmittance T_{total}, integrating the forward scattering and the direct beam. This is different from the example of TEMPO oxidized nanocellulose film (Fig. 1), or turbidimetry on suspension for which only the direct beam was taken in to account. When the forward scattering is integrated as transmission, τ_{total} is representing the elimination of the high-angle scattering, which would include Rayleigh scattering and reflection.

Using the transmission data published as figure by Chen et al. (2019), I plotted the τ_{total} normalized with sample thickness against λ^{-2} (Fig. 6a and d,) Indeed the values roughly overlap confirming the linear relation over the large wavelength. Furthermore, a linear slope can be seen for non-acetylated transparent wood sample, indicative of thin scatterer in the sample. However, the y-intercept is much higher than the wavelength-dependent part, indicating that the major contribution to the attenuation is not wavelength dependent, and thus is not Rayleigh scattering. The acetylated wood did not show linear curve, so the τ_{total} was further plotted as function of λ^4 in Fig. 6e. It still shows convex slope but now the Rayleigh scattering contribution is more significant than the non-acetylated sample.

The regular transmission can be calculated from the published data of T_{total} and the hase H as $T = T_{\text{total}}(1-H)$. However, the optical thickness $\tau = -\ln(T)$ normalized to the sample thickness τ/t was systematically higher for thinner sample. One can consider a constant surface scattering contribution. Figs. 6c and g plots $(\tau - const)/t$ against λ^{-2} that roughly shows overlapping curve for all samples, with linear dependence on λ^{-2}. The detail of surface preparation is not described, but the sawn wood surface might be rough if not plained and cause scattering. Since this surface contribution is not apparent in the τ_{total}, the surface is mostly contributing to the forward scattering.

7. Conclusions

Light scattering, if quantitatively analyzed, can guide us to understand the structure and the origin of apparent optical properties of transparent wood and wood products. The concept of static light scattering could be applied to analyze both transparent nanopaper and transparent wood.

Conflict of Interest

There are no conflicts to declare.

References

Bohren, C.F., Huffman, D.R., 1983. Absorption and Scattering of Light by Small Particles. Wiley, New York.
Carr, M.E., Hermans, J., 1978. Size and density of fibrin fibers from turbidity. Macromolecules 11, 46–50.
Chen, H., Baitenov, A., Li, Y., Vasileva, E., Popov, S., Sychugov, I., Yan, M., Berglund, L., 2019. Thickness dependence of optical transmittance of transparent wood: chemical modification effects. ACS Appl. Mater. Interfaces 11, 35451–35457.
Debye, P., 1944. Light scattering in solutions. J. Appl. Phys. 15, 338–342.
Guinier, A., Fournet, G., 1955. Small-Angle Scattering of X-rays. Structure of Matter Series. Wiley Chapman and Hall, New York.
Iyer, K.R.K., Neelakantan, P., Radhakrishnan, T., 1968. Birefringence of native cellulosic fibers. I. Untreated cotton and ramie. J. Polym. Sci. A 6, 1747–1758.
Li, Y.Y., Fu, Q.L., Yu, S., Yan, M., Berglund, L., 2016. Optically transparent wood from a nanoporous cellulosic template: combining functional and structural performance. Biomacromolecules 17, 1358–1364.
Rayleigh, L., 1899. On the transmission of light through an atmosphere containing small particles in suspension, and on the origin of the blue of the sky. Lond. Edinb. Dublin Philos. Mag. J. Sci. 47, 375–384.
Shimizu, M., Saito, T., Fukuzumi, H., Isogai, A., 2014. Hydrophobic, ductile, and transparent nanocellulose films with quaternary alkylammonium carboxylates on nanofibril surfaces. Biomacromolecules 15, 4320–4325.
Shimizu, M., Saito, T., Nishiyama, Y., Iwamoto, S., Yano, H., Isogai, A., Endo, T., 2016. Fast and robust nanocellulose width estimation using turbidimetry. Macromol. Rapid Commun. 37, 1581–1586.
Swanepoel, R., 1983. Determination of the thickness and optical constants of amorphous silicon. J. Phys. E: Sci. Instrum. 16, 1214–1222.
Tanaka, R., Kuribayashi, T., Ogawa, Y., Saito, T., Isogai, A., Nishiyama, Y., 2017. Ensemble evaluation of polydisperse nanocellulose dimensions: rheology, electron microscopy, X-ray scattering and turbidimetry. Cellulose 24, 3231–3242.
Vasileva, E., Chen, H., Li, Y.Y., Sychugov, I., Yan, M., Berglund, L., Popov, S., 2018. Light scattering by structurally anisotropic media: a benchmark with transparent wood. Adv. Opt. Mater. 6, 1800999.